minerals

MDPI

Article

Studies on the Enrichment Feasibility of Rare Earth-Bearing Minerals in Mine Tailings

Jose L. Corchado-Albelo [1] and Lana Alagha [1,2,*]

[1] Mining Engineering and Explosives Engineering Department, Missouri University of Science and Technology, Rolla, MO 65409, USA
[2] Thomas J. O'Keefe Institute for Sustainable Supply of Strategic Minerals, Missouri University of Science and Technology, Rolla, MO 65409, USA
* Correspondence: alaghal@mst.edu; Tel.: +1-(573)-341-6287

Abstract: This study aimed to investigate the potential of enrichment of rare-earth-bearing minerals in historic mine tailing using the froth flotation process. Characterization studies indicated that tailings contained 11,000 ppm of rare earth elements (REEs). The major mineral in the tailings was apatite at ~84%, which was associated with iron oxides (~16%). TESCAN's integrated mineral analysis (TIMA) showed that monazite was the main REE mineral, and 69% of monazite was locked in apatite grains. Characterization studies suggested that the separation of REEs-bearing apatite from iron oxides is possible using froth flotation, wherein apatite was floated and iron oxides were depressed. Zeta potential experiments were conducted to understand the behavior of the main minerals in the feed when selected depressants of iron oxides were added. Depressants included corn starch, sodium metasilicates, polyacrylamide (PAM), hybrid polyacrylamide (HyPAM), and chitosan. Zeta potential results suggested that chitosan and polyacrylamide-based polymers had the strongest adsorption on magnetite at pH 7 and pH 9, respectively, as indicated by the large shift in the zeta potential of magnetite suspensions. Flotation results were consistent with zeta potential findings and showed that Hy-PAM and chitosan had the best depression efficiency of iron oxides at pH 9 and pH 7, respectively.

Keywords: rare earth elements; froth flotation; phosphate minerals; TESCAN's integrated mineral analysis (TIMA); chitosan

Citation: Corchado-Albelo, J.L.; Alagha, L. Studies on the Enrichment Feasibility of Rare Earth-Bearing Minerals in Mine Tailings. *Minerals* **2023**, *13*, 301. https://doi.org/10.3390/min13030301

Academic Editors: Mostafa Benzaazoua and Yassine Taha

Received: 16 December 2022
Revised: 3 February 2023
Accepted: 14 February 2023
Published: 21 February 2023

1. Introduction

Critical minerals (CM) have become the foundation of several technologies and have been extensively used in many industries, such as modern electronics, green energy, healthcare, transportation, and defense [1–3]. Due to the increased vulnerability of supply chains and the need for a secure domestic supply, many nations have generated lists of critical minerals highlighting elements or commodities that represent a high supply risk to their specific national production and security [4–7]. The representative elements in these lists are based on commodity demand, shortage, political tensions, environmental implications, and strategic applications [1–7].

Among all the critical minerals lists, a common group deemed "critical" are rare earth elements (REEs). REEs are defined as a group of 17 elements comprised of lanthanide elements in addition to scandium and yttrium. REEs are the most prevalent critical minerals because they have become an indispensable resource for their applications in many rapidly expanding industry sectors including complex electronics, healthcare hardware, catalysis, metallurgy, renewable energy, and transportation and defense optimizations. To address the supply risk challenge surrounding REEs, an increased desire for research in abandoned mine tailings sites has been coupled with the interest in national remediation and sustainable mineral processing strategies [8]. However, mine tailings are low-grade resources that need selective strategies for enrichment. Therefore, profound sampling scale and characterization strategies are required to successfully implement sustainable mineral

processing strategies. In addition, detailed characterization helps determine suitable processing routes for metallurgical processing. For example, in the Mountain Pass mine in the U.S., which produces REE concentrates from bastnaesite processing, the mineralogy of the resource allows beneficiation by froth flotation practices [9].

Beneficiation of REE-bearing minerals is usually achieved using a combination of different separation techniques. These techniques include size reduction and screening, electrostatic and magnetic separation, gravity concentration, and froth flotation [10]. In the case of lower-grade resources, most beneficiation strategies involve the use of the froth flotation process [11,12]. Froth flotation is a fundamental technology for processing low-grade, refractory ores and possibly mine tailings with complex mineralogy because of the ability to selectively adjust parameters and modify minerals 'surface characteristics to target a specific mineral/metal of interest. Froth flotation is also a sustainable environmental practice compared to other processes, especially with the innovative developments in materials science research that allow for the design of more efficient and green reagents [13–15]. This development is beneficial from both economic and environmental perspectives. It improves selectivity and process kinetics, reduces reagent consumption, and could significantly reduce the cost of post-processing tailings management. However, developing robust flotation flowsheets to target REEs in mine tailings requires a comprehensive understanding of their complex mineralogy [16].

Several previous studies discussed the use of froth flotation with other physical separation methods for REEs' beneficiation [17–26]. For example, Satur et al. [17] studied the flotation of REE carbonates and phosphates from low-grade silicate/hematite ore at different process parameters using fatty-acid-based collectors with different depressant combinations. Their results indicated that the recoveries of REEs and gangue oxides were ~80% and ~30% on average, respectively, when fatty acids collectors were used with sodium lignin sulfonate, sodium metasilicate, sodium fluoride, or soluble starch used as depressants at pH 7–11.5 [17,18]. Bench-scale flotation on heavy mineral sands containing REEs showed that a high recovery of REEs (~95%) was achieved using fatty-acid-based and phosphoric acid ester collectors with a sodium silicate depressant [19,20]. The commercial beneficiation of REEs has also been reported in the literature. For example, at Mountain Pass, California, USA, and Mount Weld mine in Australia, flotation is employed to enrich rare earth oxides (REO) from 3%–15% to 40%–60% in concentrates [9,17]. The Bayan Obo mine in China uses magnetic separation and froth flotation to concentrate the REO feed grade from 6 to 65% [11,21,22]. In general, fatty acids and hydroxamates are the most common collectors used in the flotation of REE minerals; however, different depressant schemes must be used on a deposit basis to selectively target the gangue minerals present [19,24]. For example, depression of zircon from monazite using sodium oleate collector, sodium metasilicate depressants at elevated temperature, and pH 10 provided the highest overall recovery at 95% of total REEs [25]. However, beneficiation strategies for low-grade REEs deposits are still in development, and to the best of the authors' knowledge, there are no commercial routes for their production. Therefore, this research looked into using the froth flotation process to enrich REEs in low-grade mine tailings.

The main goals of this research were to assess and evaluate the REEs contents and mineralogy in mine tailings, followed by investigations on the possible physical enrichment of REE-bearing minerals. First, tailings were comprehensively characterized using X-ray diffraction analysis (XRD), X-ray fluorescence analysis (XRF), inductively coupled plasma mass spectrometry (ICP-MS), and TESCAN's Integrated Mineral Analysis (TIMA). Then, zeta potential measurements were conducted to evaluate the potential of different organic and inorganic reagents to serve as effective depressants of iron oxides. Zeta potential could provide insight into the selectivity of the reagent's adsorptions at mineral/water interfaces, which would help to understand the behavior of the major minerals in the flotation feed. Lastly, bench-scale flotation tests were conducted using the selected depressants. The proposed depressants were polyacrylamide (PAM), in-house-synthesized hybrid polyacrylamide (HyPAM), chitosan, sodium silicates, and corn starch. Moreover, TIMA studies on

the concentrate and tailing products were performed to obtain an in-depth understanding of the deportment of REE minerals during the flotation process.

The reagents proposed in this work are commonly and abundantly used as processing agents in mineral separation processes, including froth flotation [27–30]. For example, polyacrylamide-based (PAM) polymers were successfully tested as effective depressants of iron minerals [31,32]. On the other hand, HyPAM has been used as a sorbent and flocculant in many applications due to its unique structural characteristics [33,34]. Furthermore, chitosan polymer is known for its effectiveness as an adsorbent of iron in water treatment plants [35–37] and has been successfully applied as an effective depressant of iron minerals in the sulfide flotation process [13,38,39]. For example, Hayat et. al. [38] obtained 60% separation efficiency between galena and pyrite when polymetallic sulfide ore of the Mississippi Valley type (MVT) was floated with chitosan at 50 g/t and pH 8. Chitosan has also been used as an effective depressant of silicates in the phosphate flotation process [40].

2. Materials and Methods

2.1. Tailings and Model Minerals

Tailing samples were collected from a historic mining tailings district in Missouri, U.S. Iron oxide minerals (primarily magnetite and hematite) were the principal ores processed at this mining district [41]. The samples were air-dried and sieved. Pure apatite and magnetite samples used for zeta potential measurements were purchased from Ward's Science; the apatite [$Ca_5(PO_4)_3(OH)$] was sampled from Massive PK/10, Madagascar, whereas the magnetite was sampled from LS Ishpeming, MI, USA.

2.2. Flotation Reagents

Sodium oleate used as a phosphate collector was purchased from TCL America™ (10 g/L stock solution). Sodium metasilicate, corn starch, PAM, and chitosan used as depressants for iron oxides were purchased from Fisher Scientific, Pfaltz & Bauer, and Alfa Aesarand, respectively. All depressants were prepared in 1 g/L of stock solution. Sodium hydroxide and hydrochloric acid used for pH modification were prepared as 1 M solutions and were purchased from ACROS organics and Fisher Scientific, respectively. In-house-synthesized hybrid polyacrylamide (HyPAM) was prepared according to procedures described in the literature [28,30,42].

2.3. Grain Size Analysis/Sieve Analysis

U.S.-Mesh sieves 100 (150 µm), 120 (125 µm), 200 (75 µm), 230 (63 µm), and 400 (38 µm) were used to perform grain size analyses following ASTM C-136 protocols. The staked sieves were placed in a Combs Gyratory sifting Machine to aid the grain size separation. All other factors, such as sieving time and mass per shaker run, were determined following protocols designated in ASTM C-136 [43,44]. Particle size fraction 200 mesh (−75 µm) to 400 mesh (+38 µm) was used for zeta potential experiments. Particle size fraction 120 mesh (−125 µm) to 230 mesh (+63 µm) was used for characterization and batch flotation tests. The samples were dried overnight in a laboratory drying oven when wet sieving was used to remove the clay-size sediments.

2.4. Induced Coupled Plasma–Mass Spectrometry Analyses

The inductively coupled plasma mass spectrometry (ICP-MS) was performed to assay minor and trace elements in the flotation feed sample. ICP-MS analytical services were conducted at Geoscience Laboratories and Activation Laboratories, Canada. Samples for ICP-MS analysis were prepared using closed vessel multi-acid-digestions. The closed vessel digestion (SOL-CAIO) data obtained from the ICM-100 method was the most accurate in measuring elemental quantities of acid-resistant phases, such as REEs-bearing minerals (monazite and apatite). The expected accuracy for the ICP-MS apparatus used was ±10–30%. To powder the sample for closed vessel acid digestion, an agate mill was used to reduce the particle sizes to pass a 75 µm sized sieve, and the powdered sample was then

dried in a vacuum-sealed oven for SOL-CAIO. The sample was prepared at a standard ICP-100 dilution, and for custom inductively coupled mass spectrometry (IMX-CUS), at a five-time dilution for the heavy rare earth element values [45,46].

2.5. X-ray Diffraction Studies

The X-ray diffraction analyses (XRD) were performed using a Philips high-intensity ceramic sealed tube that works within the Cu Kα (1.5405 Å) X-ray source. The software used to analyze was the Phillips X'Pert suite. The XRD was used for semiquantitative analysis of phase analysis of powdered samples.

2.6. X-ray-Fluorescence Studies

The Energy Dispersive X-ray Fluorescence Spectroscopy (XRF) assays were performed to identify the main mineral phases in the tailings sample. The samples were analyzed in an Oxford Instruments X-Supreme 8000 XRF using a 5-sample carrousel for pelleted powdered samples.

2.7. TESCAN's Integrated Mineral Analysis Studies

TESCAN's Integrated Mineral Analysis (TIMA) was performed to identify the mineral associations and locking behavior for different REEs-bearing mineral phases. TIMA was conducted at Montana Technological University's Center for Advanced Materials Processing (CAMP) using a polished epoxy mount containing the tailings sample. Using TIMA software, the sample was prepared for automated phase analysis by scanning electron microscopy-energy dispersive X-ray (SEM-EDS) and backscattered electron (BSE) analysis.

2.8. Zeta Potential Measurements

Zeta potential measurements were conducted using Zetasizer Nano by Malvern Instruments, Inc. Mineral suspensions for the zeta potential measurements were prepared using a −38 µm size fraction at 0.1 wt.% in distilled water. The mineral suspensions were agitated using an IKA C-MAG stirrer for three minutes. After agitation, the suspensions were placed in an ultrasonic cleaning bath for approximately five minutes. Next, the pH modifiers were added as needed, followed by the addition of reagents at predetermined dosages. The suspensions were further agitated for 3 min and allowed to settle overnight to reduce cloudiness. The supernatants were used to measure the zeta potential.

2.9. Batch Flotation Experiments

Batch flotation tests were carried out in a Denver D1 flotation machine with the 1L cell and the 2–7/8″ diameter impeller attachment [17,36–39]. The flotation feed (−125 to +63 µm) was prepared in tap water at 40 wt.% solids. The prepared slurry was agitated at 1200 RPM for 4-min, and the slurry's pH was modified as needed using NaOH. Sodium oleate was used as a collector for phosphate minerals at a dosage of 350 g/t, and MIBC was used as a frother at a dosage of 17.5 g/t. Reagents used as depressants for iron oxide minerals included sodium metasilicate, chitosan, HyPAM, and PAM. The depressants' dosage was fixed at 500 g/t unless otherwise stated [47]. Experiments using chitosan only as an iron oxide depressant were conducted using 20 wt. % solids and chitosan's dosage was changed from 50 to 500 g/t.

Concentrates were collected over 4 min of flotation time. The concentrate and tailing products were dried, weighed, and assayed using XRD and XRF. Recovery was calculated using Equation (1). The grade of phosphates in the feed and flotation concentrates was expressed in terms of phosphorus pentoxide (P_2O_5).

$$\% \text{ Recovery } (R) = \frac{Cc}{Ff} \times 100 \quad (1)$$

where C is the mass of the concentrates, c is the wt.% P_2O_5 in the concentrates, F is the mass of the feed, and f is the wt.% P_2O_5 in the feed.

3. Results

3.1. Characterization Studies

The tailings samples used in this study were obtained from an abandoned mine in Missouri, U.S. The main commodity historically produced in that mine was iron oxides. Grain size analysis for the as-received tailings shows a P_{80} distribution of 100 µm and a P_{50} (median) distribution of 69 µm (Figure 1). Preliminary XRD analysis of the tailing samples indicated that the two major mineral classes in the tailings were phosphate and iron oxide minerals. As reported in the literature, in direct flotation of phosphate minerals, the optimum size of the flotation feed is −100 +75 µm [48]. Based on the modal analysis of different size fractions for phosphates and iron oxide minerals shown in Corchado 2021, a size fraction of −125 to +63 µm was selected for consequent characterization studies and flotation experiments [49,50].

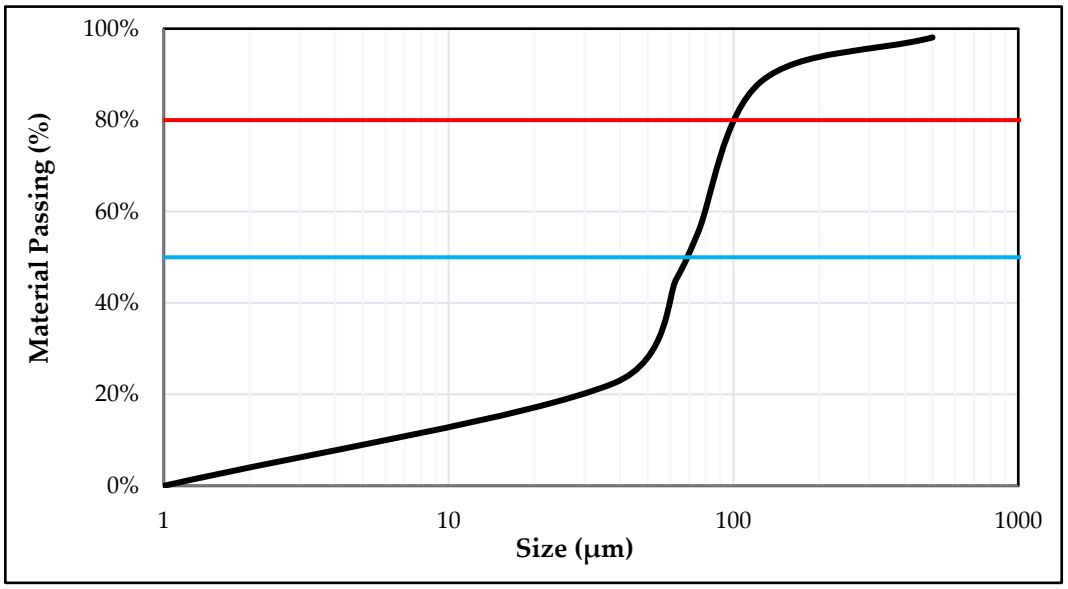

Figure 1. Grain size analysis of the as-received tailings.

The concentrations of rare earth elements (REEs) in the flotation feed (size fraction −125 to +63 µm), determined using ICP-MS, are shown in Table S1 (Supplementary Information). The major REEs were cerium at 3170 ppm, lanthanum at 1670, yttrium at 2233 ppm, and neodymium at 1380 ppm. Additionally, the flotation feed had a higher concentration in light REEs (7200 ppm) than in heavy REEs (3200 ppm). The total REEs (TREEs) concentration in the flotation feed was ~11,000 ppm [51].

Powder XRD and XRF analyses were performed on the flotation feed. XRD results (Figure S1, Supplementary Information) showed that the feed contained 84% fluorapatite, 10% hematite, and 6% quartz. XRF results (Table S2, Supplementary Information) showed that P_2O_5 and CaO accounted for 65 wt.% of the feed due to the presence of apatite in the sample. As shown in Table S2, the content of SiO_2 and Fe_2O_3 was ~30 wt.%.

TIMA's particle size distribution (PSD) analysis of the flotation feed showed a P_{80} of 108 µm, while the P_{50} (median) was 74 µm. TIMA showed that apatite was the major mineral at 69% (Figure 2). The gangue minerals were iron oxides (hematite/magnetite) at 18%, quartz at 5%, K-feldspar at 2.3%, and fluorite at 0.7%. TIMA indicated that the total oxides/hydroxides content was ~18% (primarily iron oxides and silicates). The sample also contained 1.1% phyllosilicates, 0.9% sulfates, 0.7% fluoride, 0.5% carbonates, and 0.1% sulfides.

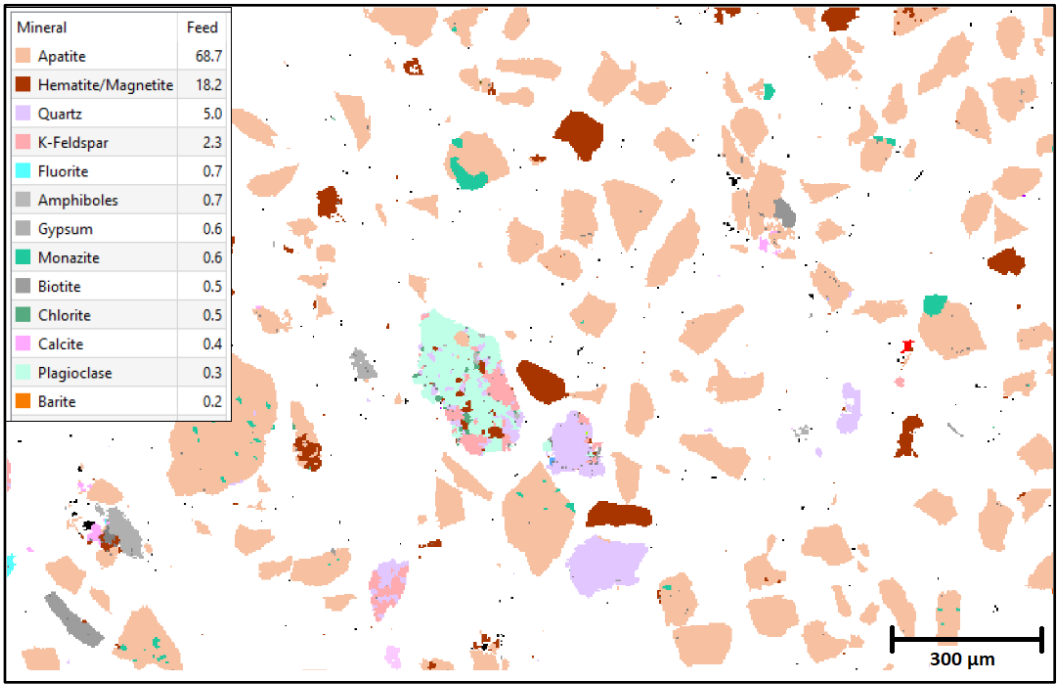

Figure 2. False-color TIMA image shows mineral associations in the flotation feed. Monazite (blue-green) is seen as large grains attached primarily to apatite grains.

As revealed by TIMA, REE minerals accounted for 0.64% of the flotation feed. Monazite [(Ce,La,Nd)PO_4] was the major REE mineral at 0.60%, and xenotime [YPO_4] was the next most abundant REE mineral at 0.02%. The other REE minerals were synchysite [$Ca(Ce,La,Nd)(CO_3)_2F$], parsite [$Ca(Ce,La,Nd)_2(CO_3)_3F_2$], and allanite [$(Ca,Ce)_2(Al,Fe)_3(SiO_4)(Si_2O_7)O(OH)$].

Additionally, the sample consisted of 0.19% cerium, 0.12% lanthanum, 0.01% yttrium, and dysprosium, ytterbium, and gadolinium at trace levels of less than 0.01%. As shown in Table 1, approximately 97% of cerium, lanthanum, and neodymium in the sample were hosted in monazite. REEs distribution data shown in Table 1 were obtained using TIMA software, which automatically quantified all detectable REE phases using mean atomic mass data and used that information to calculate the modal abundance of REE minerals and individual rare earth element abundance [52].

Table 1. Distribution of major REEs within the dominant REE minerals in the flotation feed as revealed by TIMA.

Mineral	Cerium (%)	Lanthanum (%)	Neodymium (%)
Monazite	96.9	96.7	97.3
Synchysite	1.7	1.8	1.7
Parisite	0.9	0.9	1
Allanite	0.5	0.6	T [1]
Total	100	100	100

[1] trace amounts <0.1%.

Additionally, the liberation and locking behavior of REE minerals determined using TIMA software are shown in Table 2 and Figures S2–S4 (Supplementary Information). Monazite was mainly locked in apatite grains, as seen in Table 2 and Figures S2 and S3. The locking behavior of monazite minerals showed that it was locked at 69.7% within apatite, 3.1% within hematite/magnetite, 1.9% within quartz, 1.2% within gypsum, 0.5% within calcite, 0.3% within k-feldspars, and 0.3% within chlorite.

Table 2. Monazite liberation and locking behavior within different minerals in the flotation feed as revealed by TIMA.

Mineral	Feed (%)
Apatite	69.7
Hematite/Magnetite	3.1
Quartz	1.9
Gypsum	1.2
Calcite	0.5
K-Feldspar	0.3
Chlorite	0.3
Free Surface	22.4

Table 3 shows the mineral associations of all detected REE minerals in the flotation feed. As shown, there was a strong association of monazite and xenotime with apatite. For example, monazite was 77.5% associated with apatite and 5.7% with iron oxides. Xenotime showed a 77.9% association with apatite and a 12.4% association with iron oxides. Synchysite and parisite were primarily associated with apatite at 65.7% and 82.4%, respectively. Allanite was strongly associated with quartz at 60.7%. The low percentage of the free particle is generally related to the liberation and locking analysis, which indicated that monazite and secondary REE minerals were not well liberated. This low liberation suggested that the phosphate flotation process could be a feasible strategy to enrich REE minerals that were locked in apatite. Overall, TIMA results suggested a complex mineralization of REE minerals in the flotation feed.

Table 3. Mineral associations of REE minerals in the flotation feed as revealed by TIMA.

Mineral	Monazite (%)	Synchysite (%)	Parisite (%)	Allanite (%)	Xenotime (%)
Apatite	77.5	4.7	3.3	0.2	77.9
Hematite/Magnetite	5.7	65.7	82.4	0.1	12.4
Quartz	3.3	8.4	1.6	60.7	3.2
Chlorite	1.7	0	0	17.6	0.6
Monazite		5	5.9	0.1	2.1
Amphiboles	0	0	0	5.2	0.1
K-Feldspar	0.1	0	0	4.4	0.3
Free particles	7.5	14.8	6.6	11.7	3.1

3.2. Zeta Potential Experiments

Zeta potential tests were conducted to investigate the electrical characteristics of the main minerals in the flotation feed (i.e., apatite and magnetite) at different pH points and to gain insight into the adsorption selectivity of the selected organic and inorganic depressants on magnetite surfaces.

Figure 3 shows the zeta potential (ζ) values of apatite and magnetite suspensions at three pH points: pH 4, pH 7, and pH 9 before mixing with the different depressants. At pH 4, both apatite and magnetite surfaces were positively charged, and a large difference in zeta potential values was observed where ζ values of apatite and magnetite were +4.41 mV and +21.3 mV, respectively. The positive surface charge of apatite at acidic pH may be due to the formation and precipitation of positively charged calcium ion complexes ($CaOH^+$) on apatite surfaces [53]. In the case of magnetite, at acidic pH, when excess protons exist, the dominant species is tentatively $Fe(II,III)OH_2^+$ which will render the surface charge positive [54]. However, at acidic pH, apatite could also generate OH^- in addition to $CaOH^+$, which should decrease the magnitude of the positive charge compared to magnetite [53,55].

At pH 7 and 9 (optimal pH for phosphate flotation), the ζ values of apatite and magnetite suspensions were comparable. For example, at pH 7, the ζ values of apatite and magnetite suspensions were −17.3 mV and −20.3, respectively, whereas, at pH 9, the ζ values of apatite and magnetite suspensions were −23.9 and −25.3, respectively. The

results of zeta potential measurements are consistent with those previously reported in the literature [53,54,56]. The similarities of the surface charges of apatite and magnetite at pH 7 and 9 indicated that the untreated mineral surfaces were anticipated to have similar interactions with the flotation collector during the froth flotation process. Therefore, an effective magnetite depressant is needed for enhanced separation of apatite from magnetite.

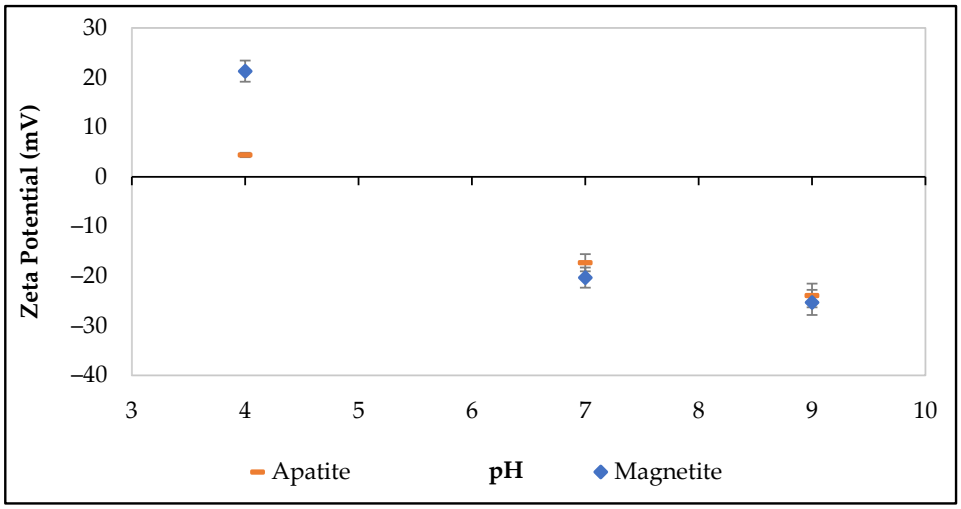

Figure 3. Zeta Potential measurements for apatite and magnetite suspensions at pH 4, 7, and 9.

Figure 4 shows the zeta potential measurements of magnetite suspensions after the addition of the selected depressants: Sodium metasilicate, corn starch, PAM, HyPAM, and chitosan at pH 4, 7, and 9 to examine the impact of depressants' adsorption on the surface charge of magnetite as a function of pH and to assess the adsorption selectivity in terms of the change in the magnitude of zeta potential ($\Delta\zeta$) after depressant's adsorption.

As shown, chitosan's addition caused the largest shift of zeta potential ($\Delta\zeta$) of magnetite suspensions at pH 4 and pH 7, which suggested that chitosan had the strongest interaction with magnetite surfaces compared to other depressants at these pH points. The measured $\Delta\zeta$ of magnetite suspensions after chitosan's addition was +18.2 mV and +32.4 mV at pH 4 and 7, respectively. Chitosan is anticipated to adsorb on the surface of magnetite minerals via the chelation mechanism between the amide and hydroxyl groups of chitosan and the iron metal of magnetite [57]. The iron-chitosan chelation mechanism has been intensively studied in the medical field as it is used to remove excess iron in the bloodstream [58]. However, the weak chelation affinity of chitosan at pH 9 was likely due to the poor solubility of the polymer at alkaline pH [59,60]. This solubility issue of chitosan limited its ability to interact with the mineral surface and thus resulted in a smaller $\Delta\zeta$ at pH 9 compared with pH 4 and 7.

PAM-based polymers had significant adsorption on the magnetite's surface at pH 7 and pH 9. The measured $\Delta\zeta$ of magnetite's suspensions with PAM at pH 7 and pH 9 were +17.2 mV and +12.5 mV, respectively, whereas, with HyPAM, $\Delta\zeta$ were +13.7 mV and +10.4 mV, respectively. The interaction of polyacrylamides with magnetite minerals could be due to polar colloidal interactions between -COOH groups of PAM molecules and Fe^{3+} ions on the magnetite's surface [61–63].

Commercially used depressants, sodium metasilicate, and corn starch showed similar $\Delta\zeta$ when added to magnetite suspensions. Sodium metasilicate and corn starch showed a $\Delta\zeta$ of −4.0 mV and −3.6 mV at pH 4, +13.7 mV and +13.8 mV at pH 7, and +1.2 mV and +2.5 mV at pH 9 of, respectively. The interaction between the magnetite's surface and these commercial depressants was likely due to electrostatic interactions [47,64–66].

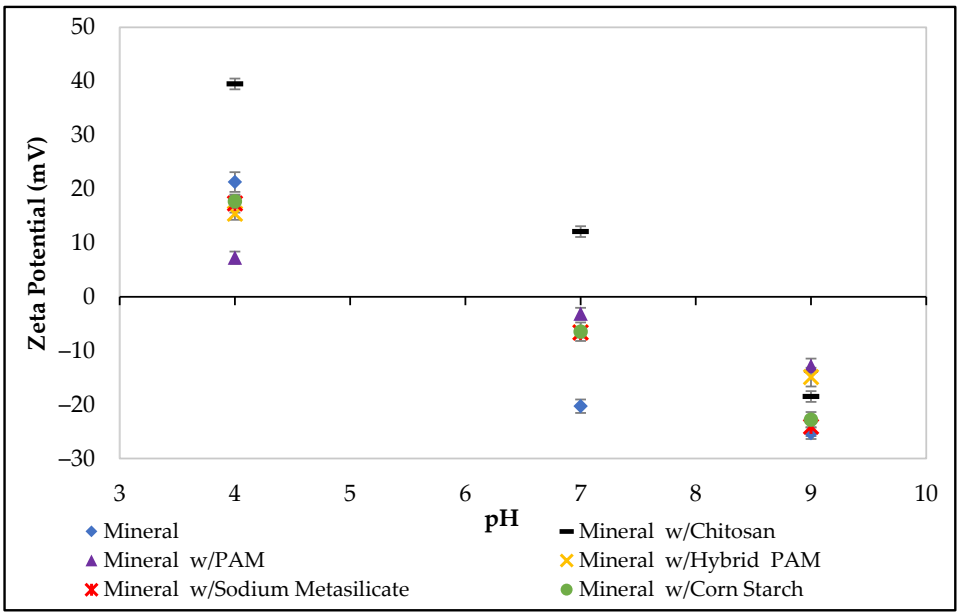

Figure 4. Zeta potential measurements of magnetite suspensions with the selected depressants at pH 4, 7, and 9.

Zeta potential results showed that chitosan had strong adsorption on iron oxides' surface at pH 7 and outperformed all other depressants tested. Results were consistent with those previously reported in the literature [50].

3.3. Batch Flotation Studies

This set of experiments was conducted at pH 9 to mimic industrial practices used for apatite flotation since sodium oleate (collector) has been shown to have a better selectivity towards phosphate minerals' surfaces at pH 9 and above [17,40,41]. The flotation efficiency of phosphate minerals in the presence of selected iron oxide depressants is shown in Figure 5. The flotation feed had a phosphate grade (given as wt.% P_2O_5) of 25 wt.%. Figure 5 shows that the highest recovery of P_2O_5 was 30% and was observed with HyPAM. The results showed that the selected depressants impacted the flotation recovery of P_2O_5 in the following order: HyPAM > chitosan > PAM > sodium metasilicate (SM) > corn starch (C). Figure 5 shows the highest grade of P_2O_5 was 29 wt.% obtained when sodium metasilicate and chitosan were used as an iron oxide depressant. Commercial depressants (sodium metasilicate and corn starch) were expected to perform better at high dosages; however, the possibility of slime coatings of clay minerals in the feed could have negatively impacted the recovery of phosphate minerals [33,67].

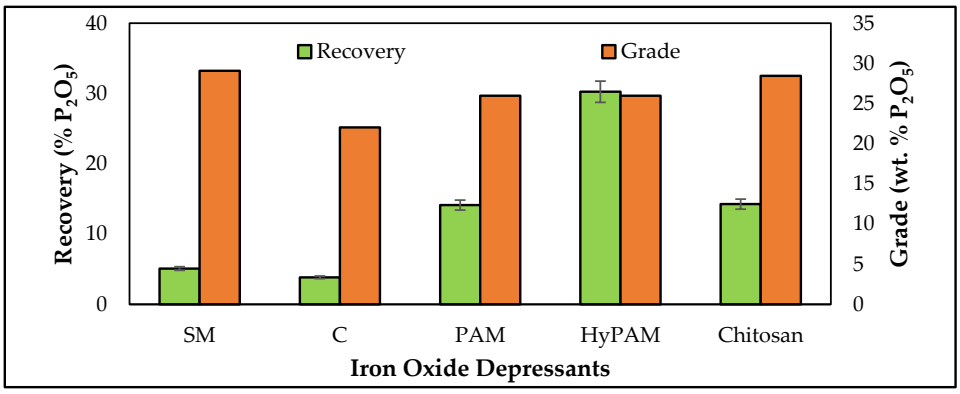

Figure 5. Recoveries and grades of P_2O_5 in the flotation concentrates when selected iron oxide depressants were used at 500 g/t and pH 9.

Results from the flotation tests suggested that flotation recovery was higher when chitosan, HyPAM, or PAM were utilized. The preferential adsorption of polymeric depressants on magnetite's surface was also identified in the zeta potential experiments. Comparing the batch flotation and zeta potential result at pH 9, for example, showed that polyacrylamide-based reagents had stronger interactions with magnetite surfaces than corn starch and sodium silicate.

Overall, the recoveries of phosphate minerals observed in the batch flotation studies at pH 9 were generally low, which suggested further investigations were necessary. Since the zeta potential results revealed that chitosan was the most selective depressant for magnetite at pH 7, detailed studies on the flotation of tailing samples with the chitosan polymer were performed using various chitosan dosages at pH 7. The flotation efficiency of phosphate minerals (presented as wt.% P_2O_5) in tailing as a function of chitosan dosage (varied from 50 to 500 g/t) is shown in Figure 6.

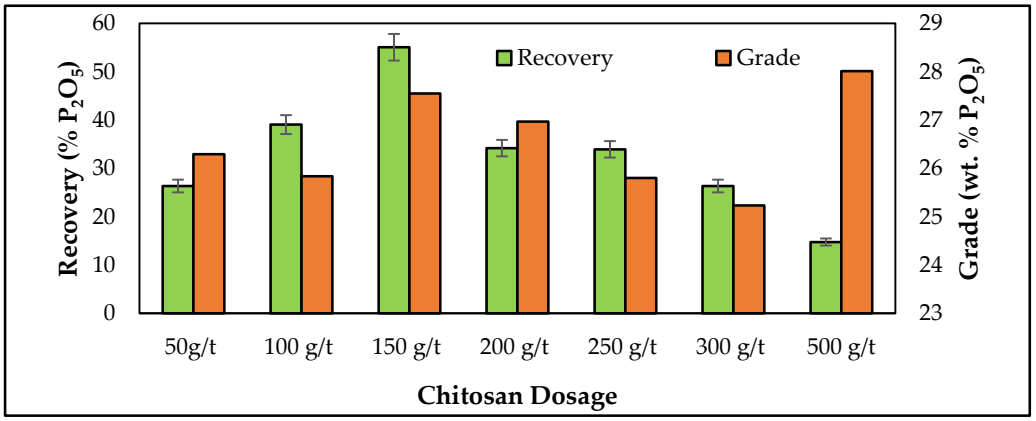

Figure 6. Recoveries and grades of P_2O_5 in the flotation concentrates when chitosan was used as a depressant at different dosages and pH 7.

The best flotation efficiency of phosphate minerals was achieved at 150 g/t of chitosan, where 55% of phosphates were recovered at a grade of 27 wt.%. The highest P_2O_5 grades were 27 wt.% and 28 wt.% obtained at 150 g/t and 500 g/t, respectively. Additionally, the high % recovery values of P_2O_5 indicated that chitosan adsorbed on iron oxide minerals at a higher rate than on phosphate minerals in the feed, which was consistent with zeta potential measurements and the previously reported data on the high efficacy of chitosan in removing iron in wastewater treatment [37]. To obtain a fundamental understanding of the deportment of REE minerals during the flotation process, concentrate and tailings products produced at the optimum chitosan dosage (150 g/t) were further analyzed using TIMA.

3.4. Deportment Studies on REE Minerals in Flotation Products

As mentioned in the previous section, TIMA studies on concentrates and tailing products were sought to understand the distribution behavior of REE minerals in flotation products (i.e., concentrates and tailings) while observing the consistency of the postulated link between phosphates (mainly apatite) with REEs. TIMA results (Table S3, Supplementary Information) showed that the total content of REE minerals in the concentrates and tailings was 0.67 wt.% and 0.58 wt.%, respectively. The main REE mineral was monazite in both the flotation concentrate and tailing samples, followed by xenotime (0.01 wt.%). Apatite grains were highlighted as the most abundant mineral in concentrates and tailings at 74 wt.% and 64 wt.%, respectively. The flotation tailings also reported 22 wt.% of iron oxides, while the concentrates showed only 15 wt.% iron oxides.

Additionally, TIMA liberation and locking analysis were performed to validate the assumption that the locking behavior of monazite (a representative of the REE minerals) to larger apatite grains was maintained in the flotation concentrates and tailings. Monazite grains were fine, with 81% being less than 10 µm and 96% less than 20 µm. The monazite

grain size distribution P_{80} was larger in the flotation concentrate at 50 µm compared to 31 µm in the tailing; however, the median for both was 15 µm. For the locking/liberation analysis, monazite was primarily locked within apatite at~ 72% and~ 60% in the tailings and concentrates, respectively (Table 4). Monazite-free particles amounted to 23% in tailing and 29% in concentrate. Thus, the liberation of monazite was low in both samples while being slightly better for the concentrate sample.

Table 4. Mineral liberation of monazite in flotation tailings and concentrates.

Mineral	Tailing	Concentrate
Apatite	71.8	59.8
Hematite/Magnetite	1.3	4.9
Quartz	2.4	2.7
Gypsum	0.8	0.9
K-Feldspar	0.1	0.8
Calcite	0.3	0.3
Fluorite	0	0.5
Free surface	22.9	29.4

Mineral associations of REE minerals in the flotation concentrates and tailings are shown in Tables 5 and 6. As shown, monazite was primarily associated with apatite in the concentrates and tailings at 67.3% and 78.8%, respectively. Monazite was also found associated with iron oxide minerals at 11.8% and 1.3% in the concentrates and tailings, respectively. The secondary REE mineral, xenotime, showed 80% and 40.8% association with apatite in the concentrates and tailings, respectively. Xenotime also showed a 53% association with iron oxide minerals in the tailings compared to 5.6% in the concentrates, which suggested that xenotime lost to tailing was due to the depression of iron oxides when chitosan was added. Synchysite was 68% associated with chlorite in concentrates and 100% associated with free particles in the tailings. Parisite was 75% associated with monazite in the concentrates and 93.3% associated with free particles in the tailings. Allanite was 73.4% associated with free particles in the concentrates and 77.4% with garnets (other garnet minerals reported in the tailings).

Overall, the TIMA characterization results showed that >70% of REE minerals in the tailings were locked in apatite minerals. Therefore, using standard phosphate flotation procedures to enrich the mine tailings was inefficient. Results suggested that optimizing the froth flotation parameters and implementing further pre-concentration strategies could be beneficial to reducing the apatite loss to tailings and could result in higher enrichment of REEs in flotation concentrates. Therefore, the researchers proposed the flowsheet shown in Figure 7 for future attempts to enrich REEs from phosphate mine tailings.

Table 5. Mineral associations of REE minerals in flotation concentrates as revealed by TIMA (Chitosan was used as a depressant at 150 g/t).

Mineral (%)	Monazite	Synchysite	Parisite	Allanite	Xenotime
Monazite		1.3	75	0	2.6
Synchysite	1.2		0	0	0
Parisite	0.2	0		0	0
Allanite	0	0	0		0
Xenotime	0	0	0		
Apatite	67.3	0	25	20.2	80
Hematite/Magnetite	11.8	0	0	0	5.6
Quartz	4.7	0	0	0	3.5
Gypsum	2.4	0	0	0	0
Calcite	1	0	0	4.9	0
Chlorite	0	68	0	0	0
Garnet	0	30.7	0	0	0.7
Free particles	10.6	0	0	73.4	7.6

Table 6. Mineral associations of REE minerals in flotation tailings as revealed by TIMA (Chitosan was used as a depressant at 150 g/t).

Mineral (%)	Monazite	Synchysite	Parisite	Allanite	Xenotime
Monazite		0	1.6	0	0.06
Synchysite	0		0	0	0
Parisite	0	0		0	0
Allanite	0	0	0		0
Xenotime	0	0	0	0	
Apatite	78.8	0	3.1	0.6	40.8
Quartz	4.3	0	0	0	3.8
Gypsum	2.2	0	0	0	0
Hematite/Magnetite	1.3	0	0.3	0	53
Amphiboles	0	0	0	9.9	0
Chlorite	0	0	1.8	6	0
Garnet	0	0	0	77.4	0
Free Particles	12.8	100	93.3	4.5	0.3

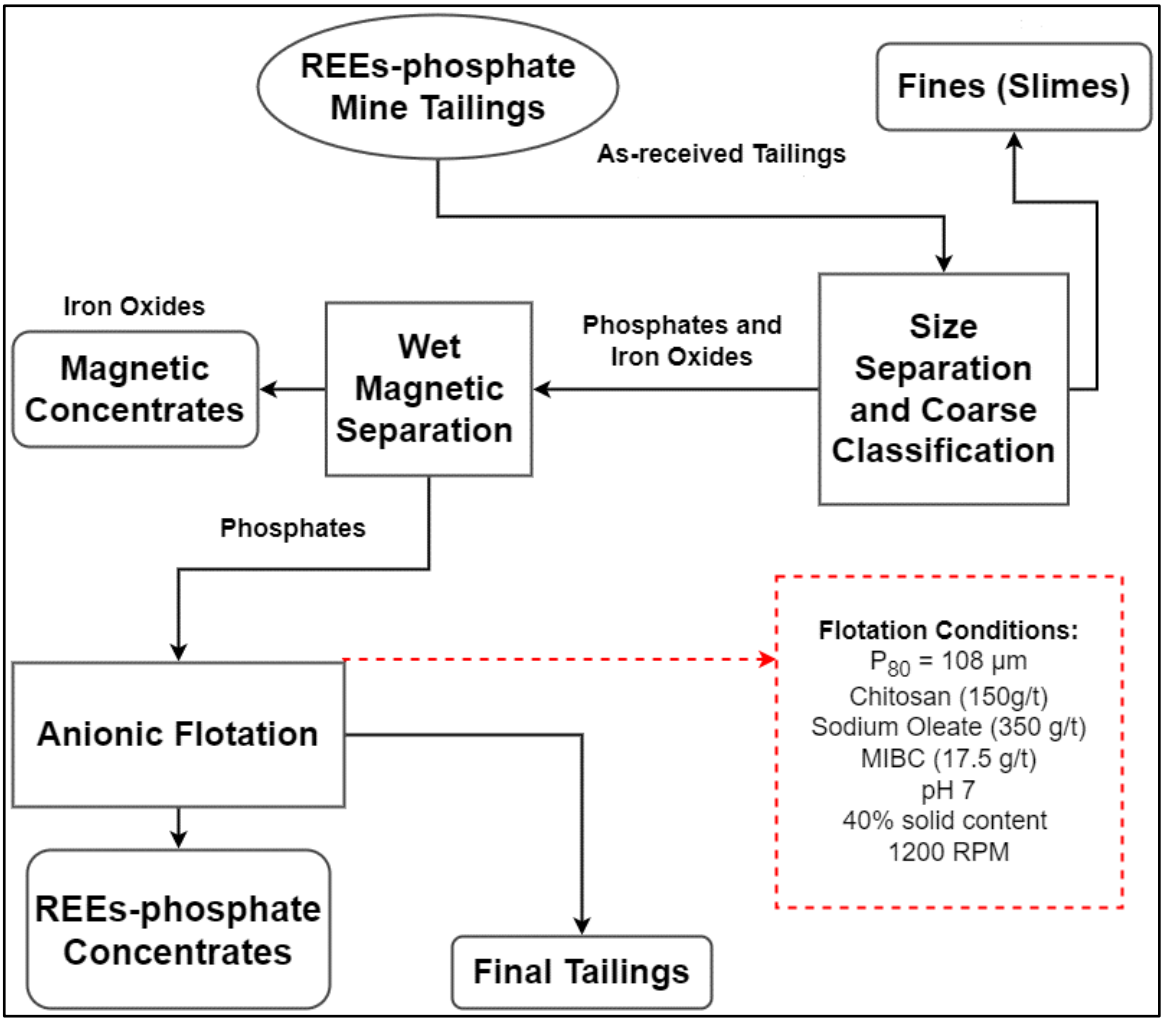

Figure 7. Proposed flotation flowsheet for the enrichment of REE-bearing phosphates in tailings.

4. Conclusions and Outlook

Characterization studies of the mine tailing samples indicated that the tailings contained a high concentration of both heavy and light REEs. Extensive studies on mineralogy showed a large abundance of apatite, followed by iron oxides (magnetite/hematite), quartz, and calcite as gangue minerals. The total concentration of REEs, as determined by ICP-MS,

was ~11,000 ppm. TIMA characterization studies also confirmed that ~70% of REE minerals were locked within apatite grains. The REE minerals locked to apatite suggested that the froth flotation process of phosphate minerals was a feasible approach to enrich REEs.

Zeta potential studies suggested that chitosan had the strongest adsorption on magnetite's surfaces at pH 7 as indicated by the large shift in the zeta potential values of magnetite suspensions after chitosan's addition. Zeta potential tests also suggested that at pH 9, polyacrylamide-based reagents had the strongest adsorption on magnetite's. Findings from the batch flotation studies performed using the selected iron oxide depressants suggested that HyPAM, PAM, and chitosan outperformed the commercial depressants (corn starch and sodium metasilicate). TIMA studies on the flotation products showed that total REE minerals in the concentrates and tailings were 0.67 wt.% and 0.58 wt.%, respectively. Monazite was the major REE mineral presented, and the grains were 81% less than 10 µm. Monazite locking analysis showed strong locking within apatite at 72% and 60% in the tailings and concentrates, respectively.

In summary, the low flotation recoveries observed highlighted that the standard beneficiation procedures used in this work to enrich REE-bearing mineral phases were not optimal, especially for recovering REE locked within apatite minerals. The locking behavior of REE minerals suggested that higher-enrichment of REEs could be feasible by increasing the recovery of apatite minerals reporting to the flotation concentrates. The low recovery of apatite has raised concerns about the possible weathering of phosphate minerals in the tailing sample and/or slime coating of mineral grains that resulted in recovery loss and low enrichment. Therefore, additional fundamental studies to investigate the surface characteristics of different minerals in tailing samples are vital to develop an efficient flowsheet for REE enrichment. Moreover, additional beneficiation steps prior to the flotation process and the post-process upgrade of concentrate products must be considered to enhance the total enrichment of REE minerals.

It is worth mentioning that all samples analyzed and processed in this research were collected as grab samples. Although grab sampling is considered an easy, quick, and less expensive approach for preliminary feasibility evaluation, these grab samples cannot account for the large tailings body heterogeneity and large spatial distribution. Therefore, to address the lack of representativeness and site heterogeneity, it is necessary to pursue large-scale sampling strategies, such as those used for heavy mineral sands and placer deposits. For example, the classic drive pipe method at multiple locations can be used wherein a pipe is driven into the consolidated material specified depths to create a plug or "core" that is representative of a cross-section for that point in the large area. The cross-sectional map helps identify regions of high resource concentrations and resource-barren regions [67]. Thereafter, the data from each logged "core" are used for resource reserve estimations. Resource estimations are important to quantify the REE resource, REE- reserves, and operation economic feasibility. The economic feasibility of operations given by reserve estimation is pivotal when addressing the feasibility of the beneficiation strategies performed in this research.

Supplementary Materials: The following supporting information can be downloaded at: https://www.mdpi.com/article/10.3390/min13030301/s1, Table S1: ICP-MS analysis for REEs in the flotation feed. Table S2: X-ray fluorescence analysis (XRF) of the flotation feed. Table S3: Modal mineral concentrations in flotation tailings and concentrates (P—mineral detected at less than 0.01%). Figure S1: X-ray diffraction patterns (XRD) of the flotation feed. Figure S2: TIMA false-color image of selected monazite (blue-green) grains in the feed sample shows a strong association with apatite (peach). Figure S3: TIMA false-color image of monazite liberation by volume in the flotation feed. Monazite's locking to larger apatite grains is readily apparent in the 0% to 30% liberation. Figure S4: TIMA false-color image of selected xenotime (red) grains in the flotation feed shows a strong association with apatite (peach) and iron oxides (brown). Figure S5: False-color TIMA image shows mineral associations in the flotation concentrate (chitosan was used as a depressant at 150 g/t). Monazite (blue-green) is seen as large grains attached primarily to apatite grains. Figure S6: Selected

monazite (blue-green) grains in the flotation concentrates (chitosan was used as a depressant at 150 g/t) shows a strong association with apatite (peach) in TIMA false-color image.

Author Contributions: Conceptualization, J.L.C.-A. and L.A.; methodology, J.L.C.-A.; formal analysis, J.L.C.-A. and L.A.; investigation, J.L.C.-A.; resources, L.A.; data curation, L.A.; writing—original draft preparation, J.L.C.-A.; writing—review and editing, L.A. and J.L.C.-A.; visualization, J.L.C.-A.; supervision, L.A.; project administration, L.A. All authors have read and agreed to the published version of the manuscript.

Funding: This research received no external funding.

Data Availability Statement: The data presented in this study are available in this article and supplementary materials here.

Conflicts of Interest: The authors declare no conflict of interest.

References

1. DOE. *Critical Materials Rare Earths Supply Chain: A Situational White Paper*; DOE: Washington, DC, USA, 2020; pp. 1–21.
2. DOE. *Critical Materials Strategy*; DOE: Washington, DC, USA, 2010; pp. 1–166.
3. Peck, D. A Historical Perspective of Critical Materials, 1939 to 2006. In *Critical Materials: Underlying Causes and Sustainable Mitigation Strategies*; Erik Offerman, S., Ed.; World Scientific Publishing Co.: Hackensack, NJ, USA, 2019; Volume 5, pp. 85–101.
4. Bobba, S.; Carrrara, S.; Mathieux, F.; Pavel, C. *Critical Raw Materials for Strategic Technologies and Sectors in the EU: A Foresight Study*; EU Publications: Luxembourg, 2020; pp. 1–100. [CrossRef]
5. Agency for Natural Resources and Energy. Japan's New International Resource Strategy to Secure Rare Metals/Special Contents—Energy Japan. Available online: https://www.enecho.meti.go.jp/en/category/special/article/detail_158.html (accessed on 21 September 2021).
6. Geoscience Australia. Australia Critical Minerals. Available online: https://www.ga.gov.au/about/projects/resources/critical-minerals (accessed on 21 September 2021).
7. Australia Government | Department of Industry, Science, Energy and Resources. The Opportunity for the Critical Minerals Sector. Available online: https://www.industry.gov.au/data-and-publications/australias-critical-minerals-strategy/the-opportunity-for-the-critical-minerals-sector (accessed on 21 September 2021).
8. Seal, R.R.; Piatak, N.M. Environmental Attributes and Resource Potential of Mill Tailings from Diverse Mineral Deposit Types. In *Proceedings of the Mine Water and Circular Economy*; Wolkersdorfer, C., Sartz, L., Sillanpää MHäkkinen, A., Eds.; IMWA: Lappeenranta, Finland, 2017; pp. 603–609.
9. USGS. *USGS Rare Earths—Mineral Commodity Summaries 2020*; USGS: Reston, VA, USA, 2020.
10. Fuerstenau, M.C.; Han, K.N. *Principles of Mineral Processing*; Society for Mining, Metallurgy, and Exploration: Littleton, CO, USA, 2003; ISBN 0873351673.
11. Abaka-Wood, G.B.; Zanin, M.; Addai-Mensah, J.; Skinner, W. Recovery of Rare Earth Elements Minerals from Iron Oxide–Silicate Rich Tailings—Part 1: Magnetic Separation. *Miner. Eng.* **2019**, *136*, 50–61. [CrossRef]
12. Abaka-Wood, G.B.; Zanin, M.; Addai-Mensah, J.; Skinner, W. Recovery of Rare Earth Elements Minerals from Iron Oxide–Silicate Rich Tailings—Part 2: Froth Flotation Separation. *Miner. Eng.* **2019**, *142*, 105888. [CrossRef]
13. Monyake, K.C.; Alagha, L. Enhanced Separation of Base Metal Sulfides in Flotation Systems Using Chitosan-Grafted-Polyacrylamides. *Sep. Purif. Technol.* **2021**, *281*, 119818. [CrossRef]
14. Kyzas, G.Z.; Matis, K.A. The Flotation Process Can Go Green. *Processes* **2019**, *7*, 138. [CrossRef]
15. Dong, L.; Wei, Q.; Jiao, F.; Qin, W. Utilization of Polyepoxysuccinic Acid as the Green Selective Depressant for the Clean Flotation of Phosphate Ores. *J. Clean. Prod.* **2021**, *282*, 124532. [CrossRef]
16. Leonida, C. Froth Flotation for the 21st Century: Engineering, Geology, Mineralogy, Metallurgy, Chemistry, Etc. *Eng. Min. J.* **2019**, *220*, 58–64.
17. Satur, J.V.; Calabia, B.P.; Hoshino, M.; Morita, S.; Seo, Y.; Kon, Y.; Takagi, T.; Watanabe, Y.; Mutele, L.; Foya, S. Flotation of Rare Earth Minerals from Silicate-Hematite Ore Using Tall Oil Fatty Acid Collector. *Miner. Eng.* **2016**, *89*, 52–62. [CrossRef]
18. Abaka-Wood, G.B.; Addai-Mensah, J.; Skinner, W. Review of Flotation and Physical Separation of Rare Earth Element Minerals. In Proceedings of the 4th UMaT Biennial International Mining and Mineral Conference, Tarkwa, Ghana, 4 August 2016; Volume 4, pp. 55–62.
19. Jordens, A.; Cheng, Y.P.; Waters, K.E. A Review of the Beneficiation of Rare Earth Element Bearing Minerals. *Miner. Eng.* **2013**, *41*, 97–114. [CrossRef]
20. Andrews, W.H.; Collins, D.N.; Hollick, C.T. The Flotation of Rare Earths-A Contribution to Industrial Hygiene. In *The Mineral Industry in New Zealand: Proceedings of the AusIMM Annual Conference*; AusIMM: Rotorua, New Zealand, 1990.
21. Pradip. The Surface Properties and Flotation of Rare-Earth Minerals. Ph.D. Thesis, University of California, Berkeley, CA, USA, 1981.
22. Anderson, C.D.; Taylor, P.R.; Anderson, C.G. Rare Earth Flotation Fundamentals: A Review. In *IMPC 2016: XXVIII International Mineral Processing Congress Proceedings*; Canadian Institute of Mining, Metallurgy and Petroleum: Montreal, QC, Canada, 2016; pp. 1–15.

23. Zhang, B.; Liu, C.; Li, C.; Jiang, M. A Novel Approach for Recovery of Rare Earths and Niobium from Bayan Obo Tailings. *Miner. Eng.* **2014**, *65*, 17–23. [CrossRef]
24. Jordens, A.; Sheridan, R.S.; Rowson, N.A.; Waters, K.E. Processing a Rare Earth Mineral Deposit Using Gravity and Magnetic Separation. *Miner. Eng.* **2014**, *62*, 9–18. [CrossRef]
25. Pavez, O.; Peres, A.E.C. Effect of Sodium Metasilicate and Sodium Sulphide on the Floatability of Monazite-Zircon-Rutile with Oleate and Hydroxamates. *Miner. Eng.* **1993**, *6*, 69–78. [CrossRef]
26. Cheng, T.W.; Holtham, P.N.; Tran, T. Froth Flotation of Monazite and Xenotime. *Miner. Eng.* **1993**, *6*, 341–351. [CrossRef]
27. Yu, Y.; Ma, L.; Cao, M.; Liu, Q. Undefined Slime Coatings in Froth Flotation: A Review. *Miner. Eng.* **2017**, *114*, 26–36. [CrossRef]
28. Alagha, L.; Wang, S.; Xu, Z.; Masliyah, J. Adsorption Kinetics of a Novel Organic-Inorganic Hybrid Polymer on Silica and Alumina Studied by Quartz Crystal Microbalance. *J. Phys. Chem. C* **2011**, *115*, 15390–15402. [CrossRef]
29. Nanda, D.; Mandre, N.R. Mechanism of Polymeric Adsorption in Selective Flocculation of Low-Grade Iron Ore. *Sep. Sci. Technol.* **2021**, *56*, 68–77. [CrossRef]
30. Molatlhegi, O.; Alagha, L. Ash Depression in Fine Coal Flotation Using a Novel Polymer Aid. *Int. J. Clean Coal Energy* **2016**, *05*, 65–85. [CrossRef]
31. Khodakarami, M.; Alagha, L. High-Performance Polymers for Separation and Purification Processes: An Overview. *Polym.-Plast. Technol. Eng.* **2017**, *56*, 2019–2042. [CrossRef]
32. Wang, L. The Use of Polyacrylamide as a Selective Depressant in the Separation of Chalcopyrite and Galena. Master's Thesis, University of Alberta, Edmonton, AB, Canada, 2013.
33. Alsafasfeh, A.; Alagha, L. Recovery of Phosphate Minerals from Plant Tailings Using Direct Froth Flotation. *Minerals* **2017**, *7*, 145. [CrossRef]
34. Alsafasfeh, A.; Khodakarami, M.; Alagha, L.; Moats, M.; Molatlhegi, O. Selective Depression of Silicates in Phosphate Flotation Using Polyacrylamide-Grafted Nanoparticles. *Miner. Eng.* **2018**, *127*, 198–207. [CrossRef]
35. Lü, T.; Zhang, S.; Qi, D.; Zhang, D.; Zhao, H. Enhanced Demulsification from Aqueous Media by Using Magnetic Chitosan-Based Flocculant. *J. Colloid Interface Sci.* **2018**, *518*, 76–83. [CrossRef]
36. Rinaudo, M. Chitin and Chitosan: Properties and Applications. *Prog. Polym. Sci.* **2006**, *31*, 603–632. [CrossRef]
37. Sarode, S.; Upadhyay, P.; Khosa, M.A.; Mak, T.; Shakir, A.; Song, S.; Ullah, A. Overview of Wastewater Treatment Methods with Special Focus on Biopolymer Chitin-Chitosan. *Int. J. Biol. Macromol.* **2019**, *121*, 1086–1100. [CrossRef] [PubMed]
38. Hayat, M.B.; Alagha, L.; Sannan, S.M. Flotation Behavior of Complex Sulfide Ores in the Presence of Biodegradable Polymeric Depressants. *Int. J. Polym. Sci.* **2017**, *2017*, 4835842. [CrossRef]
39. Monyake, K.; Alagha, L. Depression of Pyrite in Polymetallic Sulfide Flotation Using Chitosan-Grafted-Polyacrylamide. In Proceedings of the MineXchange 2020 SME Annual Conference and Expo, Phoenix, AZ, USA, 23–26 February 2020.
40. Alsafasfeh, A.; Alagha, L.; Alzidaneen, A.; Nadendla, V.S.S. Optimization of Flotation Efficiency of Phosphate Minerals in Mine Tailings Using Polymeric Depressants: Experiments and Machine Learning. *Physicochem. Probl. Miner. Process.* **2022**, *54*, 150477. [CrossRef]
41. Ovanic, J. Mining Operations at Pea Ridge Iron Ore Company—A Case Study. In *Underground Mining Methods*; Hustrulid, W.A., Bullock, R.L., Eds.; SME, Inc.: Littleton, CO, USA, 2001; pp. 229–234.
42. Yang, W.Y.; Qian, J.W.; Shen, Z.Q. A Novel Flocculant of Al(OH)3-Polyacrylamide Ionic Hybrid. *J. Colloid Interface Sci.* **2004**, *273*, 400–4005. [CrossRef]
43. *E276-13*; Standard Test Method for Particle Size or Screen Analysis at No. 4 (4.75-Mm) Sieve and Finer for Metal-Bearing Ores and Related Materials. ASTM International: West Conshohocken, PA, USA, 2013.
44. *C136/C136M-19*; Standard Test Method for Sieve Analysis of Fine and Coarse Aggregate. ASTM International: West Conshohocken, PA, USA, 2006.
45. Geo Labs. 2022 Geoscience Laboratories Schedule of Fees and Services. *Geosci. Lab.* **2022**, *13*, 12–13.
46. Actlabs. Geochemistry Schedule of Services & Fees 2023 International. *Actlabs* **2023**, *8*, 9–11. Available online: https://actlabs.com/geochemistry/ores-concentrates-and-commodities/commodities/ (accessed on 21 September 2021).
47. Qi, G.W.; Parentich, A.; Little, L.; Warren, L. Selective Flotation of Apatite from Iron Oxides. *Int. J. Miner. Process.* **1992**, *34*, 83–102. [CrossRef]
48. Alsafasfeh, A. Recovery of Phosphate Minerals from Plant Tailings Using Direct Froth Flotation Process. Master's Thesis, Missouri University of Science and Technology, Rolla, MO, USA, 2017.
49. Corchado, J. Characterization and liberation analysis of rare earth elements inclusions within the apatite-rich tailing from the pea ridge iron mine. In *Proceedings of the GSA Connects 2021*; The Geological Society of America: Portland, OR, USA, 2021.
50. Corchado, J.; Alagha, L. Enrichment of Rare Earth Bearing Phosphates in Mine Tailings by Froth Flotation Process. In *Proceedings of the 17th International Conference on Mineral Processing and Geometallurgy, Virtual, 21 October 2021*; Velásquez, C., Gutiérrez, L., Eds.; Gecamin: Santiago, Chile, 2021; pp. 1–10.
51. Corchado-Albelo, J.L.; Alagha, L. Assaying rare earth elements within the apatite-rich tailing from the pea ridge iron mine for froth flotation processing. In *Proceedings of the SME Annual Meeting, Salt Lake City, UT, USA, 2 March 2022*; SME, Inc.: Salt Lake City, UT, USA, 2022; pp. 1–8.
52. Hrstka, T.; Gottlieb, P.; Skála, R.; Breiter, K.; Motl, D. Automated Mineralogy and Petrology—Applications of TESCAN Integrated Mineral Analyzer (TIMA). *J. Geosci.* **2018**, *63*, 47–63. [CrossRef]

53. Somasundaran, P. Zeta Potential of Apatite in Aqueous Solutions and Its Change during Equilibration. *J. Colloid Interface Sci.* **1968**, *27*, 659–666. [CrossRef]
54. Sun, Z.-X.; Su, F.-W.; Forsling, W.; Samskog, P.-O. Surface Characteristics of Magnetite in Aqueous Suspension. *J. Colloid Interface Sci.* **1998**, *197*, 151–159. [CrossRef] [PubMed]
55. Zhou, F.; Liu, Q.; Liu, X.; Li, W.; Feng, J.; Chi, R.A. Surface Electrical Behaviors of Apatite, Dolomite, Quartz, and Phosphate Ore. *Front. Mater.* **2020**, *7*, 35. [CrossRef]
56. Zhao, X.; Meng, Q.; Yuan, Z.; Zhang, Y.; Li, L. Effect of Sodium Silicate on the Magnetic Separation of Ilmenite from Titanaugite by Magnetite Selective Coating. *Powder Technol.* **2019**, *344*, 233–241. [CrossRef]
57. Wang, Y.; Li, B.; Yu, Z.; Jia, D. In Situ Mineralization of Magnetite Nanoparticles in Chitosan Hydrogel. *Nanoscale Res. Lett.* **2009**, *4*, 1041–1046. [CrossRef] [PubMed]
58. Yilmaz, E. *Chitosan: A Versatile Biomaterial*; Hasirci, N., Hasirci, V., Eds.; Springer: Boston, MA, USA, 2004; ISBN 978-0-306-48584-8.
59. Chen, S.C.; Wu, Y.C.; Mi, F.L.; Lin, Y.H.; Yu, L.C.; Sung, H.W. A Novel PH-Sensitive Hydrogel Composed of N,O-Carboxymethyl Chitosan and Alginate Cross-Linked by Genipin for Protein Drug Delivery. *J. Control. Release* **2004**, *96*, 285–300. [CrossRef] [PubMed]
60. Zhu, L.; Bratlie, K.M. PH Sensitive Methacrylated Chitosan Hydrogels with Tunable Physical and Chemical Properties. *Biochem. Eng. J.* **2018**, *132*, 38–46. [CrossRef]
61. Peng, Y.; Xiao, J.; Deng, B.; Wang, Z.; Liu, N.; Yang, D.; Ding, W.; Chen, T.; Wu, Q. Study on Separation of Fine-Particle Ilmenite and Mechanism Using Flocculation Flotation with Sodium Oleate and Polyacrylamide. *Physicochem. Probl. Miner. Process.* **2020**, *56*, 161–172. [CrossRef]
62. Sun, W.; Long, J.; Xu, Z.; Masliyah, J.H. Study of Al(OH)3-Polyacrylamide-Induced Pelleting Flocculation by Single Molecule Force Spectroscopy. *Langmuir* **2008**, *24*, 14015–14021. [CrossRef]
63. Filho, E.; Brito, E.; Silva, R.; Streck, L.; Bohn, F.; Fonseca, J. Superparamagnetic Polyacrylamide/Magnetite Composite Gels. *J. Dispers. Sci. Technol.* **2021**, *42*, 1504–1512. [CrossRef]
64. Araujo, A.C.; Viana, P.R.M.; Peres, A.E.C. Reagents in Iron Ores Flotation. *Miner. Eng.* **2005**, *18*, 219–224. [CrossRef]
65. Guimarães, R.C.; Araujo, A.C.; Peres, A.E.C. Reagents in Igneous Phosphate Ores Flotation. *Miner. Eng.* **2005**, *18*, 199–204. [CrossRef]
66. Rao, K.H.; Dwari, R.K.; Lu, S.; Vilinska, A.; Somasundaran, P. Mixed Anionic/Non-Ionic Collectors in Phosphate Gangue Flotation from Magnetite Fines. *Open Miner. Process. J.* **2010**, *4*, 14–24. [CrossRef]
67. Molatlhegi, O.K. Studies on the Role of Organic-Inorganic Hybrid Polyacrylamides in Fine Coal Flotation Fine Coal Flotation. Master's Thesis, Missouri University of Science and Technology, Rolla, MO, USA, 2015.